Contribution from the Department of Chemistry,
University of California, Berkeley, California 94720

Reactions of a Coordinatively Unsaturated Rhodium Hydride Complex with Isocyanides. Preparation and Dynamic Behavior of $(\mu\text{-H})_2(\text{RNC})\text{Rh}_2[\text{P}(\text{O-}i\text{-Pr})_3]_4$ and $(\mu\text{-RNC})_2\text{Rh}_2[\text{P}(\text{O-}i\text{-Pr})_3]_4$

Stephen T. McKenna* and Earl L. Muetterties†

Received July 22, 1986

The reaction of the coordinatively unsaturated binuclear complex $(\mu\text{-H})_2\text{Rh}_2[\text{P}(\text{O-}i\text{-Pr})_3]_4$ with 1 equiv of an isocyanide RNC yields the monoadduct $(\mu\text{-H})_2(\text{RNC})\text{Rh}_2[\text{P}(\text{O-}i\text{-Pr})_3]_4$. These complexes adopt an unsymmetrical structure with one trigonal-bipyramidal and one square-pyramidal rhodium center. In the case of the relatively compact isocyanides with R = 4-ClC_6H_4, PhCH_2, and *n*-Bu, the isocyanide symmetrically bridges the two rhodium centers, while for larger isocyanides such as *t*-BuNC, steric interactions force the isocyanide into a position in which it is strongly associated with the trigonal-bipyramidal Rh and only weakly bonded to the other Rh. For all the monoadducts, a rapid fluxional process exchanges the Rh and P environments and generates a symmetrical time-averaged structure at room temperature. Variable-temperature $^{31}\text{P}\{^1\text{H}\}$ NMR spectroscopy was used to obtain the activation parameters for this process; the value of ΔH^* ranges from 9.7 to less than 7.7 kcal/mol, while ΔS^* is nearly zero. Treatment of $(\mu\text{-H})_2(\text{RNC})\text{Rh}_2[\text{P}(\text{O-}i\text{-Pr})_3]_4$ with additional RNC results in a complex fragmentation reaction, with the product distribution dependent upon the nature of the isocyanide. In addition to mononuclear fragmentation products, the zerovalent binuclear compound $(\mu\text{-RNC})_2\text{Rh}_2[\text{P}(\text{O-}i\text{-Pr})_3]_4$ is formed, particularly in the case of R = 4-ClC_6H_4. The compound $(\mu\text{-4-ClC}_6\text{H}_4\text{NC})_2\text{Rh}_2[\text{P}(\text{O-}i\text{-Pr})_3]_4$ crystallizes in the monoclinic space group $C2/c$ with a = 15.526 (2) Å, b = 20.351 (4) Å, c = 20.975 (3) Å, β = 94.34 (1)°, and Z = 4. Its X-ray crystal structure (R = 0.030, R_w = 0.038 for 3045 data with $I > 3\sigma$) shows a nonplanar geometry at each Rh atom with a bent pair of bridges (dihedral angle of 135.8° between the Rh_2C planes) and a Rh-Rh separation of 2.640 (1) Å. The chemistry of the isocyanide compounds is compared and contrasted with that of their CO analogue.

Introduction

As part of our interest in the fundamental chemistry of reactive transition-metal clusters, we have explored the reactivity of the series of compounds with the stoichiometry $(\text{HRhL}_2)_n$, where L or L_2 represent phosphite,[1,2] aminophosphine,[3] or diolefin[4] ligands and n = 2, 3, or 4. Much of our effort has been concentrated on one of the most stable and easily prepared members of this family, $(\mu\text{-H})_2\text{Rh}_2[\text{P}(\text{O-}i\text{-Pr})_3]_4$. As a coordinatively unsaturated species, this compound displays unusually high catalytic and stoichiometric reactivity toward a number of organic substrates, including olefins,[1] acetylenes,[5] and 1,3-dienes.[6] A common feature of these reactions is the facile interaction of organic molecules and dihydrogen with the vacant coordination sites of the rhodium dimer.

In order to understand this chemistry better, it was necessary to investigate the basic coordination chemistry of $(\mu\text{-H})_2\text{Rh}_2[\text{P}(\text{O-}i\text{-Pr})_3]_4$. In previous studies, it was observed[1] that addition of excess phosphite ligands to the compounds $\{\text{HRh}[\text{P}(\text{OR})_3]_2\}_n$ results in hydride bridge cleavage to give the five-coordinate mononuclear species $\text{HRh}[\text{P}(\text{OR})_3]_4$. By careful addition of small amounts of $\text{P}(\text{O-}i\text{-Pr})_3$ to $(\mu\text{-H})_2\text{Rh}_2[\text{P}(\text{O-}i\text{-Pr})_3]_4$, the intermediate cleavage product $\text{HRh}[\text{P}(\text{O-}i\text{-Pr})_3]_3$ can be isolated.[7] Reaction of $(\mu\text{-H})_2\text{Rh}_2[\text{P}(\text{O-}i\text{-Pr})_3]_4$ with internal acetylenes[5] gave an initial 1:1 adduct, $(\mu\text{-H})_2(\mu\text{-}\eta^2\text{-RCCR})\text{Rh}_2[\text{P}(\text{O-}i\text{-Pr}^i)_3]_4$, which rapidly underwent an insertion reaction to give the binuclear bridging vinyl complex $(\mu\text{-H})(\mu\text{-}\eta^2\text{-RC(H)=CR})\text{Rh}_2[\text{P}(\text{O-}i\text{-Pr})_3]_4$. Excess diaryl- or dialkylacetylenes react with this vinyl complex, leading to cluster fragmentation and insertion into the Rh-C bond to give $[\text{R(H)C=C(R)C(R)=C(R)}]\text{Rh}[\text{P}(\text{O-}i\text{-Pr})_3]_2$. Olefins, on the other hand, showed no detectable interaction with $(\mu\text{-H})_2\text{Rh}_2[\text{P}(\text{O-}i\text{-Pr})_3]_4$ in the absence of H_2.[1]

Reaction of $(\mu\text{-H})_2\text{Rh}_2[\text{P}(\text{O-}i\text{-Pr})_3]_4$ with carbon monoxide[8] appeared to follow the pattern of dialkylacetylenes: the formation of an initial 1:1 adduct, which then reacted further. The 1:1 adduct, $(\mu\text{-H})_2(\text{CO})\text{Rh}_2[\text{P}(\text{O-}i\text{-Pr})_3]_4$, was formulated as having a bridging CO ligand on the basis of IR (ν_{CO} = 1810 cm^{-1}) and NMR data. This compound was only characterized in solution due to difficulties in reaction conditions and isolation. A second, more stable product was observed as well, the binuclear Rh(0) complex $(\mu\text{-CO})_2\text{Rh}_2[\text{P}(\text{O-}i\text{-Pr})_3]_4$. This complex was isolated and characterized by X-ray crystallography. It is formally the result of replacement of H_2 in the initial 1:1 adduct, $(\mu\text{-H})_2(\text{CO})\text{Rh}_2[\text{P}(\text{O-}i\text{-Pr})_3]_4$, by a second equivalent of CO (Scheme I). While it was suggested that this was due to a disproportionation reaction of the 1:1 adduct, this was not substantiated. Due to the potential interest of complexes of this type, mindful of the known similarity between the coordination chemistry of

Scheme I

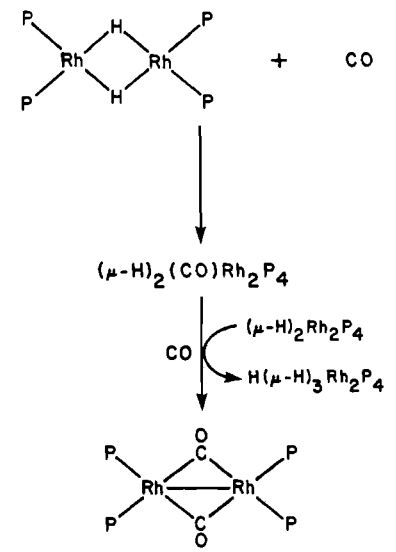

* To whom correspondence should be addressed at Amoco Chemicals Co., Naperville, IL 60566.
† Deceased Jan 12, 1984.

(1) Sivak, A. J.; Muetterties, E. L. *J. Am. Chem. Soc.* **1979**, *101*, 4878.
(2) Burch, R. R. Ph.D. Thesis, University of California, Berkeley, 1982.
(3) Meier, E.-B.; Burch, R. R.; Muetterties, E. L.; Day, V. W. *J. Am. Chem. Soc.* **1982**, *104*, 2661.
(4) Kulzick, M. A.; Price, R. T.; Muetterties, E. L.; Day, V. W. *Organometallics* **1982**, *1*, 1256.
(5) (a) Burch, R. R.; Muetterties, E. L.; Teller, R. G.; Williams, J. M. *J. Am. Chem. Soc.* **1982**, *104*, 4257. (b) Burch, R. R.; Shusterman, A. J.; Muetterties, E. L.; Teller, R. G.; Williams, J. M. *J. Am. Chem. Soc.* **1983**, *105*, 3546.
(6) Burch, R. R.; Muetterties, E. L.; Day, V. W. *Organometallics* **1982**, *1*, 188.
(7) McKenna, S. T.; Andersen, R. A.; Muetterties, E. L., manuscript in preparation.
(8) Burch, R. R.; Muetterties, E. L.; Schultz, A. J.; Gebert, E. G.; Williams, J. M. *J. Am. Chem. Soc.* **1981**, *103*, 5517.

0020-1669/87/1326-1296$01.50/0

Table I. Spectroscopic Data for $H_2(L)Rh_2[P(OPr)_3]^4$

param	L = RNC: R = 4-ClC_6H_4	R = $PhCH_2$	R = *n*-Bu	R = *t*-Bu	R = 2,6-$Me_2C_6H_3$	L = CO
			^{1}H NMR			
$\delta_{hydride}$[a]	−8.68	−8.51	−8.61	−8.67	−9.25	−9.09
J_{HP}, Hz	48.6	49.2	48.6	43.2	46.0	47.2
J_{HRh}, Hz	15.0	14.9	15.1	17.0	15.3	14.0
			^{31}P NMR			
δ_P[b]	151.1	156.8	157.5	156.9	155.6	155.8
$^1J_{PRh}$, Hz	253.3	253.0	253.8	254.5	258.2	253.7
$^3J_{PRh}$, Hz	10.5	11.0	11.0	10.6	10.8	11.6
$^4H_{PP}$, Hz	0.5	2.0	0.5	3.5	1.2	
$^2J_{RhRh}$, Hz	2.5	4.5	4.1	2.0	1.0	
			infrared[c]			
$\nu_{complex}$, cm^{-1}	1790	1780 1808[e]	1795	2090 2090[e]	1945[d]	1810
$\nu_{free\ ligand}$, cm^{-1}	2128	2155	2154	2140	2119	2143

[a] Toluene-d_8, 20 °C. [b] Downfield from H_3PO_4, toluene-d_8, 20 °C. [c] ν_{CN} or ν_{CO}; pentane or THF solution except as noted. [d] Broad; shoulders at 2080, 2025, 1905, and 1860 cm^{-1}. [e] KBr pellet.

CO and isocyanides (RNC),[9-11] we decided to explore the reactions of $(\mu\text{-H})_2Rh_2[P(O\text{-}i\text{-}Pr)_3]_4$ with isocyanides.

Results and Discussion

Formation of $(\mu\text{-H})_2(RNC)Rh_2[P(O\text{-}i\text{-}Pr)_3]_4$ (1). The reaction of $(\mu\text{-H})_2Rh_2[P(O\text{-}i\text{-}Pr)_3]_4$ with 1 equiv of an alkyl or aryl isocyanide RNC proceeds instantaneously at room temperature or −78 °C with the solution color changing from blue-green to red. From these solutions, orange or red materials with the stoichiometry $(\mu\text{-H})_2(RNC)Rh_2[P(O\text{-}i\text{-}Pr)_3]_4$ (**1a–e**: **1a**, R = 4-ClC_6H_4; **1b**, R = $PhCH_2$; **1c**, R = *n*-Bu; **1d**, R = *t*-Bu; **1e**, R = 2,6-$Me_2C_6H_3$) can be isolated.[12] These compounds are air-sensitive both in the solid state and in solution and are exceedingly soluble in nonpolar solvents, but they may be crystallized from polar solvent mixtures such as 2-propanol/acetonitrile. The ^{1}H NMR spectra at ambient temperature (Table I) show a single hydride resonance at approximately δ − 9 with quintet splitting (J_{HP} ~ 45 Hz) due to four equivalent ^{31}P nuclei and triplet splitting (J_{HRh} ~ 15 Hz) due to two equivalent ^{103}Rh nuclei ($I = {}^1/_2$, 100% abundance). This assignment is confirmed by $^1H\{^{31}P\}$ spectra, which show the hydride as a triplet. The ^{1}H spectra also show resonances due to only one type of phosphite ligand. The $^{31}P\{^1H\}$ NMR spectra of all five complexes at room temperature show resonances for only one type of phosphite, split into a doublet by ^{103}Rh, with a smaller splitting due to a distant ^{103}Rh and fine structure caused by J_{PP} and J_{RhRh}. The $^{13}C\{^1H\}$ spectra for R = $PhCH_2$ and *t*-Bu show a quintet (J_{CP} ~ 42 Hz) of triplets (J_{CRh} ~ 24 Hz) for the isocyanide carbon. The NMR data therefore suggest, in at least a time-averaged sense, a symmetrical structure, with the isocyanide and two hydrides bridging two RhP_2 units, for all five compounds.

The infrared spectra, however, suggest that the complexes are not all completely isostructural. As shown in Table I, the solution IR spectra of **1a–c** (R = 4-ClC_6H_4, $PhCH_2$, and *n*-Bu) display ν_{CN} values in a range consistent with a bridging or semibridging isocyanide. (Typical values for such species[13-21] are in the range

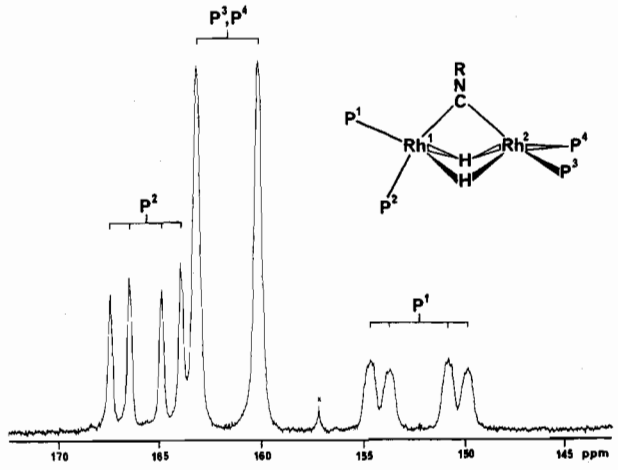

Figure 1. $^{31}P\{^1H\}$ NMR spectrum of **1c** at −105 °C, with proposed structure. For details of assignment, see text.

1650–1750 cm^{-1}, although a value of 1785 cm^{-1} was found for $Cp_2Ni_2(\mu\text{-PhNC})_2$.[14]) When R = *t*-Bu (**1d**), though, the ν_{CN} frequency of 2090 cm^{-1} is almost certainly indicative of a terminal species. For R = 2,6-$Me_2C_6H_3$ (**1e**) an intermediate value is found, but the peak is flanked by several shoulders to higher and lower energy, possibly due to the presence of a number of conformational isomers interconverting slowly on the IR time scale (but rapidly on the NMR time scale) due to the large steric bulk of the isocyanide ligand. In further support of this trend, the ^{13}C chemical shift of the isocyanide carbon of **1d** (R = *t*-Bu) is δ 155.35 while that of **1b** (R = $PhCH_2$) is δ 205.86. The former is characteristic of a terminal isocyanide, while the latter is closer to the range expected for a bridging isocyanide. (Terminal isocyanides have been observed to have ^{13}C shifts of the isocyanide carbon between about δ 140 and 185, while bridging isocyanides have been seen between about δ 207 and 257.[18-21])

Solution Structure of 1. The clue for interpreting these data can be found in the low-temperature NMR spectra of the complexes **1a-e**. The ^{1}H and ^{31}P NMR spectra of all five complexes are temperature-dependent, broadening at temperatures below

(9) Malatesta, L.; Bonati, F. *Isonitrile Complexes of Metals*; Wiley: New York, 1969.
(10) Treichel, P. M. *Adv. Organomet. Chem.* **1973**, *11*, 21.
(11) Singleton, E.; Oosthuizen, H. E. *Adv. Organomet. Chem.* **1983**, *22*, 209.
(12) The same reaction using 4-$(O_2N)C_6H_4NC$ resulted in immediate and extensive decomposition, presumably due to electron-transfer reactions.
(13) Ennis, M.; Kumar, R.; Manning, A. R.; Howell, J. A. S.; Mathur, P.; Rowan, A. J.; Stephens, F. S. *J. Chem. Soc., Dalton Trans.* **1981**, 1251.
(14) Joshi, K. K.; Mills, O. S.; Pauson, P. L.; Shaw, B. W.; Stubbs, W. H. *J. Chem. Soc., Chem. Commun.* **1965**, 181.
(15) Boylan, M. J.; Bellerby, J.; Newman, J.; Manning, A. R. *J. Organomet. Chem.* **1973**, *47*, C33.
(16) Howell, J. A. S.; Mays, M. J.; Hunt, I. D.; Mills, O. S. *J. Organomet. Chem.* **1977**, *128*, C29.
(17) Howell, J. A. S.; Mathur, P. *J. Organomet. Chem.* **1979**, *174*, 335.
(18) Howell, J. A. S.; Rowan, A. J. *J. Chem. Soc., Dalton Trans.* **1980**, 503.
(19) (a) Green, M.; Howard, J. A. K.; Spencer, J. L.; Stone, F. G. A. *J. Chem. Soc., Chem. Commun.* **1975**, 3. (b) Green, M.; Howard, J. A. K.; Murray, M.; Spencer, J. L.; Stone, F. G. A. *J. Chem. Soc., Dalton Trans.* **1977**, *1509*.
(20) Carroll, W. E.; Green, M.; Galas, A. M. R.; Murray, M.; Turney, T. W.; Welch, A. J.; Woodward, P. *J. Chem. Soc., Dalton Trans.* **1980**, 80.
(21) Bassett, J.-M.; Barker, G. K.; Green, M.; Howard, J. A. K.; Stone, F. G. A.; Wolsey, W. C. *J. Chem. Soc., Dalton Trans.* **1981**, 219.

Table II. Low-Temperature $^{31}P\{^1H\}$ NMR Data for $H_2(RNC)Rh_2[P(O\text{-}i\text{-}Pr)_3]_4$ (**1a–d**)

param[a]	**1a**, R = 4-ClC_6H_4	**1b**, R = $PhCH_2$	**1c**, R = *n*-Bu	**1d**, R = *t*-Bu
δ_{P1}	152.9	151.6	152.1	147.1
δ_{P2}	162.9	163.9	165.4	164.4
$\delta_{P3,4}$	160.6	160.5	161.4	163.4
$^1J_{P1Rh1}$, Hz	320	314	312	308
$^1J_{P2Rh1}$, Hz	211	209	208	188
$^1H_{P3,4Rh2}$, Hz	241	251	245	261
$^3J_{P1Rh2}$, Hz	21	20	20	18
$^3J_{P2Rh2}$, Hz	0	0	0	0
$^3J_{Rp,4Rh1}$, Hz	10	12	12	12
$^2J_{P1P2}$, Hz	82	79	78	70
$^4J_{P1P3,4}$, Hz	8	8	8	8
$^4J_{P2P3,4}$, Hz	−7	−4	−7	−1
temp, °C	−110	−100	−105	−114

[a] For labeling scheme, see Figure 1.

the ambient and sharpening again as low-temperature limiting spectra below approximately −100 °C. Figure 1 shows the $^{31}P\{^1H\}$ NMR spectrum of **1c** at −105 °C. This pattern is consistent with an unsymmetrical structure like that shown in the figure. The proposed structure has two inequivalent rhodium atoms. One rhodium atom (Rh1) has a trigonal-bipyramidal geometry; the axial ligands are one phosphite (P2) and the isocyanide carbon, while the equatorial ligands are another phosphite (P1) and the two bridging hydrides. The second rhodium atom (Rh_2) has a square-pyramidal geometry. The two hydrides and the remaining phosphites (P3, P4) form the basal plane, and there is an apical interaction with the isocyanide carbon. A mirror plane contains the Rh atoms, the isocyanide, P1, and P2; it makes the hydrides equivalent and P3 and P4 equivalent. From this structure, the $^{31}P\{^1H\}$ NMR spectrum can be analyzed as follows. The large doublet at δ 161, integrating as two P's, is due to P3 and P4; the splitting is due to Rh2. The doublet of doublets at δ 165, integrating as one P, is due to P2; the larger splitting is caused by Rh1 and the smaller by P1. Finally, the doublet of doublets of multiplets at δ 152 is P1, split by Rh1 and P2 with small couplings to P3, P4, and Rh2. The presence of the additional couplings in this multiplet is consistent with a phosphite in a position trans across the Rh–Rh vector from the Rh2–P3–P4 unit; P2, which is oriented cis, shows no such couplings, as expected. Complexes **1a–d** show nearly identical $^{31}P\{^1H\}$ spectra in this temperature range (see Table II); the low-temperature limiting spectrum of **1e** could not be obtained above −120 °C (vide infra).

The hydride portions of the ^1H NMR spectra of the complexes are still broad at −105 °C but in all cases show a distinct doublet character, which can be assigned as the expected large coupling to the phosphite (P3 or P4) oriented trans to each hydride across Rh2. The resonance for **1a**, which is sharper than the others, shows a further doublet splitting, with coupling constants of about 140 and 60 Hz; the smaller coupling is probably due to P1. The selectively alkyl-proton-decoupled (hydride-coupled) ^{31}P NMR spectrum of **1a** at −105 °C clearly shows the expected splitting due to the hydrides. The resonances for P3 and P4 are split into doublets by coupling to the single hydride trans to them ($^2J_{HP} \sim$ 140 Hz); no appreciable splitting is observed from the cis-oriented hydride. The pattern for P1 is further split into triplets ($^2J_{HP} \sim$ 60 Hz) by the two hydrides. There is no resolvable hydride coupling to P2, which is cis to both hydrides. Complex **1b** shows similar splittings of 143 and 63 Hz in the low-temperature hydride-coupled ^{31}P spectrum. The low-temperature ^1H and ^{31}P NMR spectra are thus totally consistent with the proposed structure.

The reasoning behind the choice of the structure in Figure 1 is as follows. The hydrides and the isocyanide are assumed to be bridging on the basis of the IR and NMR evidence presented above (at least for **1a–c**). This gives a dirhodium unit joined by three bridging ligands. Each rhodium also has two terminally bound phosphites, giving a five-coordinate geometry at each metal atom (ignoring any metal–metal interaction). This geometry can

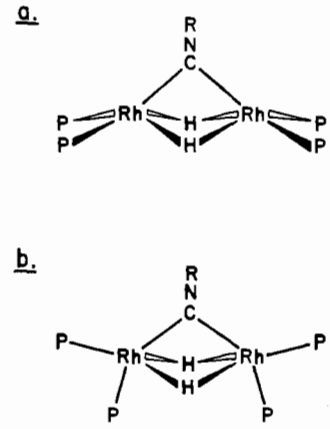

Figure 2. Two alternative structures considered in the text for compounds **1**. These and the structure in Figure 1 are the three possibilities generated by combining two five-coordinate Rh centers.

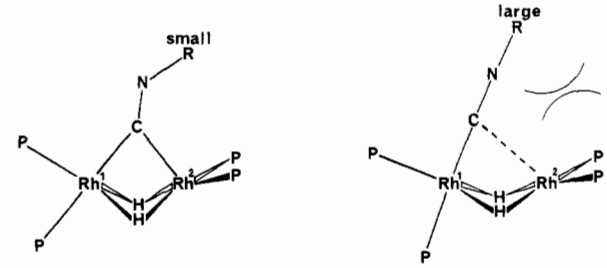

Figure 3. Comparison of structures with small (**1a–c**) and large (**1d–e**) isocyanides.

be described in terms of the two limiting five-coordinate geometries commonly observed, trigonal bipyramidal and square pyramidal. (A more precise description of the two structures is that they must be 3:2 structures of minimal C_s symmetry, imposed by the mirror plane relating P3 to P4. The two types of such structures are represented for the sake of discussion as the idealized trigonal bipyramid and square pyramid.) There are three possibilities for combining five-coordinate units: both rhodiums square pyramidal, as in Figure 2a; both trigonal bipyramidal, as in Figure 2b; an unsymmetrical geometry with one rhodium square pyramidal and one trigonal bipyramidal, as in the proposed structure of Figure 1. Only the unsymmetrical geometry could generate the observed low-temperature limiting $^{31}P\{^1H\}$ NMR spectrum; the structure of Figure 2a has only one type of phosphite, while the structure of Figure 2b has two equally populated phosphite environments. This leaves the unsymmetrical structure of Figure 1, which has the required three phosphite environments in a 1:1:2 ratio. The reason for the unsymmetrical structure is probably that, by placement of the RhP_2 groups in perpendicular planes, the large phosphite ligands can be interlocked to relieve steric strain.

The similarity of the low-temperature $^{31}P\{^1H\}$ NMR spectra of **1a–d** suggests that they all have the same basic structure. In order to explain the IR stretching frequency of the isocyanide in **1d**, which appears to show a terminal rather than bridging isocyanide, we must consider the steric factors involved. In the bridging geometry of Figure 1, the alkyl group on the isocyanide, which like all bridging isocyanides would be bent at the nitrogen, must point toward one of the rhodium atoms. The less congested position is toward the square-pyramidal Rh. Also, in cases where an isocyanide bridges two metals, it is found to be bent at N so that the alkyl group is anti to the metal to which the isocyanide is more closely bound.[21-25] In this case, bending in the proposed

(22) Adams, R. D.; Cotton, F. A.; Rusholme, G. A. *J. Coord. Chem.* **1971**, *1*, 275.
(23) Cotton, F. A.; Frenz, B. A. *Inorg. Chem.* **1974**, *13*, 253.
(24) Hunt, I. D.; Mills, O. S. *Acta Crystallogr., Sect. B: Struct. Crystallogr. Cryst. Chem.* **1977**, *B33*, 2432.
(25) Fehlhammer, W. P.; Mayr, A.; Kehr, W. *J. Organomet. Chem.* **1980**, *197*, 327.

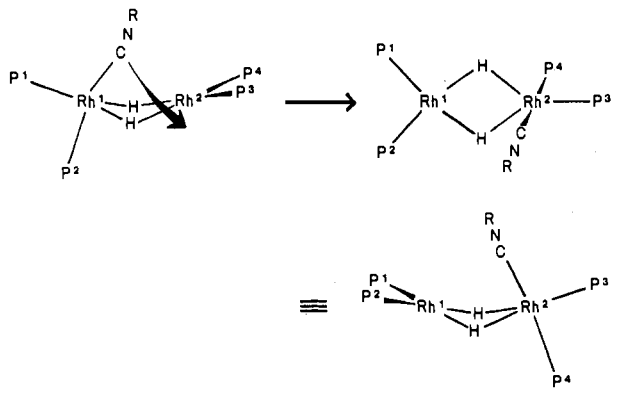

Figure 4. Proposed mechanism of fluxionality of compounds **1a–e**.

direction indicates weaker binding to Rh2, consistent with the transition between square pyramidal and 4-coordinate planar at this center. Inspections of models show that even when the bending is toward the Rh2 the steric interaction between a large isocyanide and the isopropoxide groups on P3 and P4 would be severe. The complex would respond to this steric destabilization by tilting the isocyanide away from Rh2, back to a more terminal position on Rh1, as shown in the diagram in Figure 3. This corresponds to a weakening of the apical interaction between Rh2 and the isocyanide and approaches a geometry at Rh2 that may be described as four-coordinate planar rather than square pyramidal.

This can explain both the IR and the low-temperature NMR data for all of the complexes. The gross features of the structures of **1a–e** are the same, an unsymmetrical structure like that in Figure 1. For the small isocyanides in **1a–c** (R = 4-ClC_6H_4, $PhCH_2$, and *n*-Bu), steric interactions are small enough that the isocyanide can adopt a bridging or semibridging position between the two Rh atoms. For the very bulky isocyanides in **1d,e** (R = *t*-Bu and 2,6-$Me_2C_6H_3$), however, nonbonded interactions between the isocyanide and the phosphite 2-propoxide groups force a more terminal geometry on Rh1. This can be seen in the IR spectra of the complexes. Since the symmetry and basic structures are still the same, the low-temperature NMR spectra are all similar.[26]

Dynamic NMR of 1. There remains the question of the NMR spectra observed at room temperature. As stated above, these show that all four phosphites are equivalent on the NMR time scale, as are both rhodium atoms. The hydrides and the isocyanide carbon show coupling to all four ^{31}P nuclei and to both ^{103}Rh nuclei. In order to reconcile the NMR spectra with the proposed structure, one must therefore postulate that some sort of dynamic process is responsible for averaging the phosphorus and rhodium environments.

Because of the large number of spin-$^1/_2$ nuclei in these systems, coupling patterns alone can provide much useful information about the nature of the process. In the high-temperature limit, P and Rh couplings are maintained to both the hydrides and the isocyanide carbon. Furthermore, the $^{31}P\{^1H\}$ spectra at room temperature show a strong coupling of each phosphorus to the directly bound rhodium and a weaker coupling to the distant rhodium. Selectively alkyl-proton-decoupled (hydride-coupled) ^{31}P spectra also show coupling of the phosphorus nuclei to both hydrides. This allows one to rule out any mechanism involving hydrogen, isocyanide, or phosphite dissociation, as well as any breakup of the molecules into mononuclear fragments. Any process incorporating bond-breaking steps such as these would result in the loss of coupling between the nuclei involved. Thus the dynamic process is constrained to be a wholly intramolecular one.

From the observed high-temperature limiting spectra, one can state that the dynamic process must involve motion of the isocyanide from one rhodium atom to the other. This is required

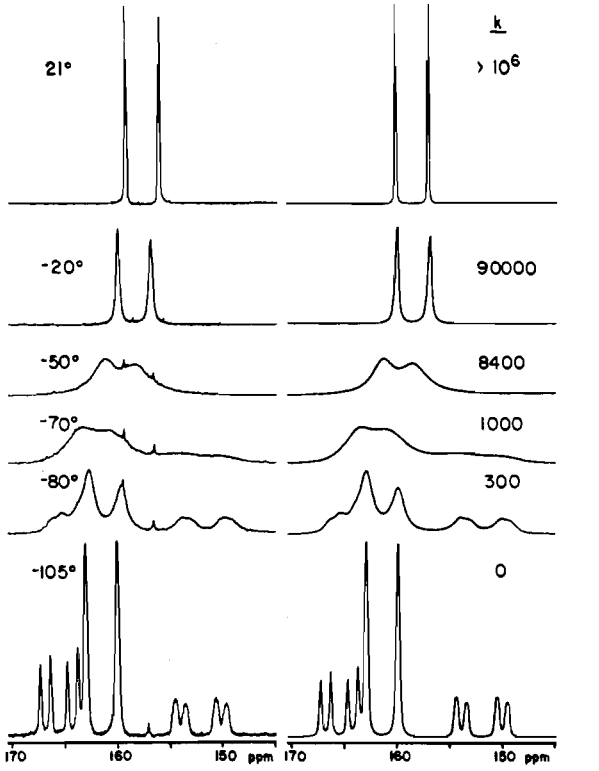

Figure 5. Variable-temperature 81.76-MHz $^{31}P\{^1H\}$ NMR spectra of **1c**: left, observed; right, calculated by using the mechanism of Figure 4 with the rate constants shown.

in order to make both Rh nuclei appear equivalent in the ^1H and $^{13}C\{^1H\}$ NMR spectra. A least-motion pathway to accomplish this is shown in Figure 4. The mechanism is best illustrated for the nearly terminal structure of **1d**, but it is applicable to all the complexes. In this mechanism, the isocyanide rotates out of the plane defined by Rh1, P1, and P2 while simultaneously moving toward Rh2, following the space separating the alkoxide groups of the two RhP_2 units. It eventually becomes predominantly bound to Rh2 and lies in the plane defined by Rh2, P3, and P4. The hydrides move so as to track the isocyanide. Figure 4 depicts a "forward" rotation of the isocyanide out of the Rh1–P1–P2 plane; a "backward" rotation, into the plane, is also possible and is required by symmetry to proceed at the same rate. Together these permutations are sufficient to average the two rhodium and three phosphorus environments into one environment each. Note that while the motion is described here as a single step, it may variously be idealized in terms of elementary steps; for example, a completely equivalent description of Figure 4 is that Rh1 and Rh2 undergo concerted turnstilelike rearrangements combined with a shift of the isocyanide.[27]

The left-hand side of Figure 5 shows the $^{31}P\{^1H\}$ spectra of **1c** at various temperatures between +21 and −105 °C. The high-temperature spectrum, a doublet of doublets due to $^1J_{PRh}$ and $^3J_{PRh}$ (slightly unsymmetrical due to the effects of $^4J_{PP}$ and $^2J_{RhRh}$) broadens and collapses as the temperature is decreased. At approximately −70 °C one sees only an unsymmetrical but otherwise featureless lump with a width of nearly 20 ppm. Upon further cooling, the spectrum reassembles into a new pattern, the low-temperature limiting spectrum shown previously in Figure 1.

The right-hand side of Figure 5 shows calculated $^{31}P\{^1H\}$ spectra based on spectral parameters derived from the high- and low-

(26) The proposed structures have been confirmed by X-ray crystallographic studies of **1b** and **1d**. The angle at the isocyanide Rh1–C–N is 134° in **1b**; it is 166° and 173° in two independent molecules of **1d**. Details of the structure determinations will be reported elsewhere: Day, V. W., manuscript in preparation.

(27) A reviewer has pointed out that this mechanism may also be described in terms of more familiar elementary steps: movement of the isocyanide to a bridging position, rupture of the Rh1–C bond, a tetrahedral to square planar arrangement at Rh1, and a turnstile-like rearrangement at Rh2 to give a trigonal bipyramid. This mechanism is equivalent to that proposed in the text if it is assumed that the rearrangements at Rh1 and Rh2 are concerted; the NMR line shapes rule out separate steps for the same reason as for the mechanism of Figure 2a (vide infra).

Table III. Activation Parameters for Fluxionality of $(\mu\text{-H})_2(\text{RNC})\text{Rh}_2[\text{P(O-}i\text{-Pr)}_3]_4$

compd	R	$\Delta H^\ddagger$, kcal/mol	$\Delta S^\ddagger$, cal/(mol K)
1a	4-ClC_6H_4	9.2 (2)[a]	5 (1)[a]
1b	$PhCH_2$	9.7 (2)	1.5 (9)
1c	*n*-Bu	8.9 (2)	−0.4 (7)
1d	*t*-Bu	7.7 (1)	−1.2 (4)
1e	2,6-$Me_2C_6H_3$	low[b]	

[a] Numbers in parentheses give least-squares estimated standard deviations of last significant digit. [b] See text.

temperature limiting spectra (see Table II) and the dynamic process illustrated in Figure 4. The fit of the calculated to the observed spectra can be seen to be quite good. Rate constants derived from the calculations can be analyzed according to the Eyring equation to give enthalpies and entripies of activation, which are shown in Table III. Results are given for the complexes **1a–d**. Values of $\Delta H^\ddagger$ fall between about 7 and 10 kcal/mol, while, to within experimental error, $\Delta S^\ddagger$ is nearly zero for all four compounds. In the case of R = 2,6-$Me_2C_6H_3$, a low-temperature limiting spectrum could not be achieved even at −120 °C. Comparison of the intermediate spectra with those of the other complexes suggested that $\Delta G^\ddagger$ was on the order of 7 kcal/mol at the coalescence temperature, but an exact value cannot be derived.

As Table III shows, the major factor affecting the enthalpy of activation is the steric bulk of the isocyanide ligand. The values of $\Delta H^\ddagger$ can be divided into two groups. For R = *n*-Bu, $PhCH_2$, and 4-ClC_6H_4, $\Delta H^\ddagger$ lies between 8.9 and 9.7 kcal/mol. For R = *t*-Bu and 2,6-$Me_2C_6H_4$, $\Delta H^\ddagger$ is 7.7 kcal/mol or less. The main reason for the break in $\Delta H^\ddagger$ does not appear to be electronic; for example, *n*-BuNC would be expected to be electronically more similar to *t*-BuNC than to 4-ClC_6H_4NC. Rather, the division between relatively low and high barriers follows the same steric trend seen in the solution structure (as judged by IR); the very large isocyanides with R = *t*-Bu and 2,6-$Me_2C_6H_3$ display a lower barrier than the other three, smaller, isocyanides. This can be rationalized by proposing that the steric demands of the transition state are less severe than those of the ground state. In this case a very bulky isocyanide would sterically destabilize the ground state relative to the transition state, thereby reducing the net barrier to fluxionality. Note that this does not contradict the earlier conclusion that large isocyanides disfavor the bridging geometry; first, the bridging environment of the isocyanide in the transition state is not the same as in the ground state of **1a–c**, and second, all that is required is that the steric destabilization of the transition state be less than that of the ground state.

A number of other mechanisms may be visualized as well. For example, one of the RhP_2 units can be allowed to twist by 90° about an axis roughly along the Rh–Rh vector to generate an intermediate or transition state with a structure like one of those previously considered and rejected as ground states in Figure 2. Both have a symmetrically bridging isocyanide between equivalent Rh atoms having local square-pyramidal or trigonal-bipyramidal geometry, respectively. Twisting one or the other RhP_2 units by ±90° then allows interconversion of isomers. The structure of Figure 2a, derived from a 90° twist of Rh1P1P2, can be ruled out since a second twist of Rh1P1P2 in the same direction results in only a net interconversion of P1 and P2, leaving all other labels unchanged. A mechanism of this type would cause the resonances for P1 and P2 to broaden faster than that for P3 and P4. The line shape simulations were found not to tolerate significant amounts of this process, either alone or in conjunction with the process in Figure 4. A process involving the structure of Figure 2b as transition state, however, can be shown to be permutationally nondifferentiable from the process in Figure 4 by the method of Klemperer;[28] that is, while not constrained to operate at the same rate, it generates the same NMR line shapes. Therefore it cannot be inferred from line shape data alone whether Figure 4 or Figure 2b represents the actual process. We prefer a concerted mechanism such as Figure 4 because it should have less steric strain than that of Figure 2b, since it does not require all the non-hydride ligands to lie in the same plane.

Scheme II

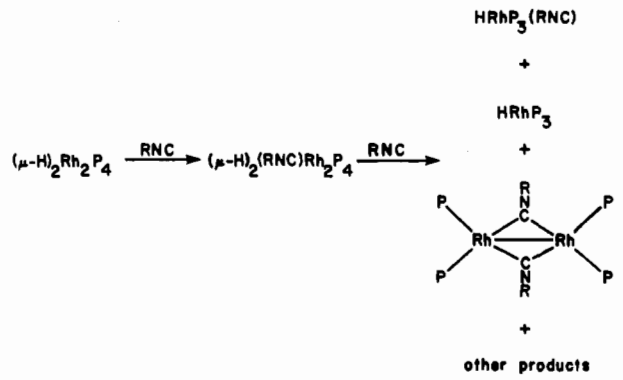

Further Reactions of 1. Complexes **1a–e** are somewhat thermally sensitive. Solutions decompose at room temperature over a period of several days, or at 70 °C over about 30 min, to yield a large number of products. The only hydride-containing decomposition product is $HRh[P(O\text{-}i\text{-}Pr)_3]_3$, formed in low yield for R = $PhCH_2$ and 4-ClC_6H_4, and identified by NMR. No isocyanide-containing products can be identified.

The addition of 1 equiv of RNC to $(\mu\text{-H})_2(\text{RNC})\text{Rh}_2[\text{P(O-}i\text{-Pr)}_3]_4$ or of 2 or more equiv of RNC to $(\mu\text{-H})_2\text{Rh}_2[\text{P(O-}i\text{-Pr)}_3]_4$ results in a mixture of products, the exact composition of which depends on the isocyanide (Scheme II). Found in all cases is $HRh[P(O\text{-}i\text{-}Pr)_3]_3(RNC)$, formed in 25–50% yield based on Rh. This compound was identified by NMR and, for R = *t*-Bu, by comparison with authentic $HRh[P(O\text{-}i\text{-}Pr)_3]_3(t\text{-BuNC})$ prepared from $HRh[P(O\text{-}i\text{-}Pr)_3]_3$[7] and *t*-BuNC. This result is analogous to that observed in the CO system,[8] where a large excess of CO generated $HRh[P(O\text{-}i\text{-}Pr)_3]_3(CO)$, $HRh[P(O\text{-}i\text{-}Pr)_3]_2(CO)_2$, and other products. (No sign of $HRh[P(O\text{-}i\text{-}Pr)_3]_2(RNC)_2$ was detected here.) $HRh[P(O\text{-}i\text{-}Pr)_3]_3(RNC)$ shows three equivalent ^{31}P nuclei in the ^1H, $^{31}P\{^1H\}$, and ^{103}Rh NMR spectra, consistent with a trigonal-bipyramidal structure with all three phosphites equatorial or with some less symmetrical structure that is fluxional on the NMR time scale. For R = 4-ClC_6H_4, $PhCH_2$, and *n*-Bu, $HRh[P(O\text{-}i\text{-}Pr)_3]_3$ was also formed in 20–45% yield. Finally, in the case of R = 4-ClC_6H_4, large amounts of $(\mu\text{-RNC})_2\text{Rh}_2[\text{P(O-}i\text{-Pr)}_3]_4$ (**2a**) were formed (the major product in this case, 44% based on Rh). A similar product with R = $PhCH_2$ (**2b**) is seen in tiny amounts (ca. 5%) for the reaction of **1b** with $PhCH_2NC$, but no such products were obtained for other isocyanides. Formally this is the result of displacement of H_2 from $(\mu\text{-H})_2(\text{RNC})\text{Rh}_2[\text{P(O-}i\text{-Pr)}_3]_4$ by RNC. It is analogous to the compound $(\mu\text{-CO})_2\text{Rh}_2[\text{P(O-}i\text{-Pr)}_3]_4$ produced in the displacement of H_2 from $(\mu\text{-H})_2(\text{CO})\text{Rh}_2[\text{P(O-}i\text{-Pr)}_3]_4$ (Scheme *I*). A number of unidentified additional products are also formed in the reactions of **1** with RNC. Thus when R = 4-ClC_6H_4 the major product is **2a**, followed by $HRh[P(O\text{-}i\text{-}Pr)_3]_3(RNC)$ and $HRh[P(O\text{-}i\text{-}Pr)_3]_3$, for R = $PhCH_2$ and *n*-Bu, mainly $HRh[P(O\text{-}i\text{-}Pr)_3]_3(RNC)$ and $HRh[P(O\text{-}i\text{-}Pr)_3]_3$ were formed, and for R = *t*-Bu, the only identifiable product was $HRh[P(O\text{-}i\text{-}Pr)_3]_3(RNC)$.

In an attempt to find an independent, more efficient synthesis of the complexes **2**, the complexes *trans*-$RhCl[P(O\text{-}i\text{-}Pr)_3]_2(RNC)$ (R = 4-ClC_6H_4, $PhCH_2$) were prepared by reaction of $(\mu\text{-Cl})_2\text{Rh}_2[\text{P(O-}i\text{-Pr)}_3]_4$[29] with 2 equiv of RNC. Various methods were tried to reduce these complexes to $(\mu\text{-RNC})_2\text{Rh}_2[\text{P(O-}i\text{-Pr)}_3]_4$. The complex *trans*-$RhCl[P(O\text{-}i\text{-}Pr)_3]_2(4\text{-}ClC_6H_4NC)$ did not react with Zn dust and reacted slowly with 1% sodium amalgam to give only decomposition products. Similarly, *trans*-$RhCl[P(O\text{-}i\text{-}Pr)_3]_2(PhCH_2NC)$ did not react with Mg powder. It did react with $KBH(O\text{-}i\text{-}Pr)_3$ in THF at −78 °C, but

(28) Klemperer, W. *J. Chem. Phys.* **1972**, *56*, 5478.

(29) Del Paggio, A. A.; Muetterties, E. L.; Heinekey, D. M.; Day, V. W.; Day, C. S. *Organometallics* **1986**, *5*, 575.

Table IV. Crystal and Data Collection Parameters for $(\mu\text{-4-ClC}_6\text{H}_4\text{NC})_2\text{Rh}_2[\text{P(O-}i\text{-Pr)}_3]_4$ (**2a**)

formula: $Rh_2Cl_2P_4O_{12}N_{C50}H_{92}$ fw: 1313.90

Crystal Parameters at 25 °C

a = 15.526 (2) Å	space group: $C2/c$ (C_{2h}^6-No. 15)[a]
b = 20.351 (4) Å	Z = 4
C = 20.975 (3) Å	d_{calcd} = 1.32 g/cm^3
β = 94.34 (1)°	μ_{calcd} = 7.18 cm^{-1}
$\alpha = \gamma$ = 90°	size: 0.42 × 0.19 × 0.18 mm

Data Measurement and Structure Solution

diffractometer: Enraf-Nonius CAD-4	scan type: θ–2θ
radiation: Mo Kα (λ = 0.710 73 Å)	2θ range: 2–45°
reflcns measd: $+h,+k,+l$	scan speed: var from 0.7 to 6.7° min^{-1}
no. of reflcs collcd (incl. stds): 4679	scan width: $\Delta\theta$ = 0.50 + 0.35tan(θ)°
no. of unique reflcs: 4314	bkgd: addnl 0.25($\Delta\theta$) at each end of scan
no. with $I > 3\sigma(I)$: 3045	final residuals:[b] R = 0.030;
no. of params: 325	R_w = 0.038; GOF = 1.38

[a] Cromer, D. T.; Waber, J. T. *International Tables for X-ray Crystallography*; Kynoch: Birmingham, England, 1974. [b] $R = (\sum||F_o| - |F_c||)/(\sum|F_o|)$, $R_w = (\sum w(|F_o| - |F_c|)^2]/[\sum wF_o^2])^{1/2}$, GOF = $(\sum w(|F_o| - |F_c|)^2]/(n_o - n_v))^{1/2}$, where n_o is the number of observations and n_v is the number of variable parameters.

Table V. Positional Thermal Parameters for $(\mu\text{-4-ClC}_6\text{H}_4\text{NC})_2\text{Rh}_2[\text{P(O-}i\text{-Pr)}_3]^4$

atom[a]	x	y	z	b,[b] Å^2
Rh	0.07828 (2)	0.17754 (2)	0.22941 (1)	3.686 (6)
Cl	−0.3927 (1)	0.0170 (1)	0.0179 (1)	13.11 (6)
P1	0.17660 (7)	0.24724 (6)	0.27925 (5)	4.47 (3)
P2	0.016385 (7)	0.12443 (6)	0.16336 (6)	5.06 (3)
O11	0.2698 (2)	0.2206 (2)	0.3015 (2)	6.23 (8)
O12	0.1941 (2)	0.3129 (2)	0.2410 (2e	6.49 (8)
O13	0.1580 (2)	0.2813 (2)	0.3459 (2)	6.75 (8)
O21	0.2633 (2)	0.1226 (2)	0.1862 (2)	6.06 (8)
O22	0.1405 (2)	0.0508 (2)	0.1449 (2)	7.66 (9)
O23	0.1738 (2)	0.1512 (2)	0.0917 (2)	7.56 (9)
N	−0.0666 (2)	0.1256 (2)	0.1354 (2)	5.14 (9)
C1	−0.0346 (2)	0.1490 (2)	0.1849 (2)	4.15 (9)
C2	−0.1468 (3)	0.1030 (2)	0.1092 (2)	5.2 (1)
C3	−0.2119 (3)	0.0855 (2)	0.1457 (2)	6.0 (1)
C4	−0.2884 (3)	0.0594 (3)	0.1174 (3)	7.5 (1)
C5	−0.2969 (3)	0.0504 (3)	0.0528 (3)	8.1 (1)
C6	−0.2339 (4)	0.0687 (4)	0.0160 (3)	10.7 (2)
C7	−0.1580 (3)	0.0960 (3)	0.0434 (3)	8.5 (2)
C111	0.3361 (3)	0.2609 (3)	0.3372 (3)	8.2 (2)
C112	0.3399 (5)	0.2412 (4)	0.4065 (4)	14.4 (2)
C1113	0.4176 (4)	0.2490 (5)	0.3078 (5)	16.9 (3)
C121	0.1937 (5)	0.3160 (3)	0.1733 (3)	10.4 (2)
C122	0.1649 (7)	0.3836 (4)	0.1543 (4)	17.2 (3)
C123	0.2803 (7)	0.3012 (5)	0.1545 (4)	17.8 (3)
C131	0.0803 (4)	0.3151 (3)	0.3581 (3)	7.5 (1)
C132	0.0650 (5)	0.3029 (4)	0.4250 (4)	12.1 (2)
C133	0.0878 (6e	0.3868 (3)	0.3436 (4)	13.1 (3)
C211	0.3294 (3)	0.0862 (3)	0.1551 (3)	7.9 (1)
C212	0.3769 (4)	0.1327 (4)	0.1147 (4)	12.9 (2)
C213	0.3868 (4)	0.0564 (4)	0.2066 (4)	11.9 (2)
C221	0.0949 (3)	0.0060 (2)	0.1849 (3)	7.1 (1)
C222	0.1569 (5)	−0.0379 (3)	0.2226 (4)	12.6 (2)
C223	0.0347 (4)	−0.0322 (3)	0.1399 (4)	10.5 (2)
C231	0.1065 (4)	0.1522 (4)	0.0440 (3)	9.8 (2)
C232	0.1136 (6)	0.2160 (5)	0.0083 (4)	15.3 (3
C233	0.1099 (8)	0.0995 (5)	−0.0009 (4)	20.5 (4)

[a] Anisotropic thermal parameters and hydrogen atom positions are given in the supplementary material. [b] B values for anisotropically refined atoms are given in the form of the isotropic equivalent thermal parameter defined as: $^4/_3[a^2B(1,1) + b^2B(2,2) + c^2B(3,3) + ab(\cos\gamma)B(1,2) + ac(\cos\beta)B(1,3) + bc(\cos\alpha)B(2,3)]$.

the result was a complex mixture from which no pure products could be isolated; the $^{31}P\{^1H\}$ NMR spectrum showed it to contain a small amount (ca. 5%) of **2b** plus some $HRh[P(O\text{-}i\text{-}Pr)_3]_3$ and $HRh[P(O\text{-}i\text{-}Pr)_3]_3(PhCH_2NC)$, but a large number of unidentified products were observed as well. Thus at this time the only convenient way to prepare pure **2a** is from $(\mu\text{-H})_2Rh_2[P(O\text{-}i\text{-}Pr)_3]_4$ by way of **1a**.

Table VI. Intramolecular Distances (Å) for $(\mu\text{-4-ClCl}_3\text{H}_4\text{NC})_2\text{Rh}_2[\text{P(O-}i\text{-Pr)}_3]_4$

Rh–Rh′	2.640 (1)	Cl–C5	1.746 (5)
Rh–P1	2.279 (1)	O11–C111	1.475 (5)
Rh–P2	2.265 (1)	O12–C121	1.420 (6)
Rh–C1	2.007 (4)	O13–C131	1.429 (6)
Rh–C1′	2.052 (4)	O21–C211	1.458 (5)
P1–O11	1.582 (3)	O22–C221	1.458 (6)
P1–O12	1.592 (3)	C23–C231	1.391 (6)
P1–O13	1.605 (3)	C111–C112	1.506 (10)
P2–O21	1.582 (3)	C111–C113	1.469 (9)
P2–O22	1.584 (3)	C121–C122	1.492 (10)
P2–O23	1.617 (3)	C121–C123	1.461 (12)
C1–N	1.215 (4)	C131–C132	1.462 (8)
N–C2	1.400 (5)	C131–C133	1.498 (8)
C2–C3	1.360 (6)	C211–C212	1.500 (9)
C3–C4	1.393 (6)	C211–C213	1.477 (8)
C4–C5	1.363 (7)	C221–C222	1.495 (8)
C5–C6	1.344 (8)	C221–C223	1.495 (7)
C6–C7	1.388 (7)	C231–C232	1.507 (11)
C7–C2	1.385 (6)	C231–C233	1.431 (10)

[a] Primed atoms are related to unprimed atoms by the crystallographic 2-fold axis.

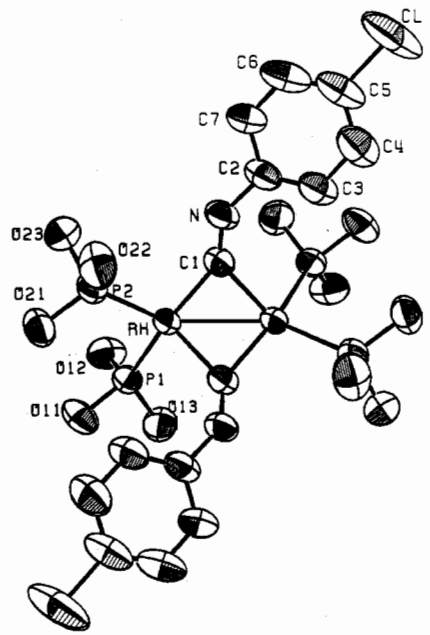

Figure 6. ORTEP diagram of $(\mu\text{-4-ClC}_6\text{H}_4\text{NC})_2\text{Rh}_2[\text{P(O-}i\text{-Pr)}_3]_4$ (**2a**). The crystallographic 2-fold axis is nearly normal to the page. The isopropyl groups on the phosphites have been omitted for clarity.

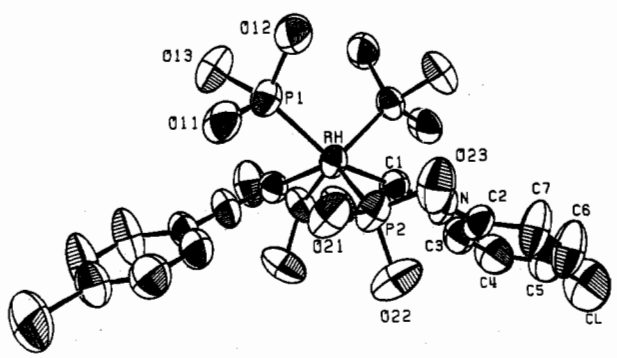

Figure 7. ORTEP diagram of **2a**. The view is directly down the Rh–Rh′ bond; the crystallographic 2-fold axis is vertical in the plane of the page.

Structure and Dynamic Behavior of 2a. An X-ray crystallographic study was performed on compound **2a**. Crystal structure parameters are given in Table IV; atomic positions and bond length

Table VII. Intramolecular Angles (deg) for $(\mu\text{-}4\text{-}ClC_6H_4NC)_2Rh_2[P(O\text{-}i\text{-}Pr)_3]_4$

P1–Rh–P2	100.02 (4)	O11–P1–O12	104.43 (16)
Rh′–Rh–P1	116.82 (3)	O11–P1–O13	96.39 (16)
Rh′–Rh–P2	142.85 (3)	O12–P1–O13	97.21 (17)
Rh′–Rh–C1	50.16 (11)	O21–P2–O22	104.60 (17)
Rh–Rh′–C1	48.69 (10)	O21–P2–O23	97.43 (17)
P1–Rh–C1	157.50 (11)	O22–P2–O23	97.32 (20)
P1–Rh–C1′	91.64 (10)	P1–O11–C111	123.2 (3)
P2–Rh–C1	96.29 (11)	P1–O12–C121	123.6 (3)
P2–Rh–C1′	130.46 (11)	P1–O13–C131	125.0 (3)
C1–Rh–C1′	89.46 (16)	P2–O21–C211	125.5 (3)
Rh–C1–Rh′	81.15 (14)	P2–O22–C221	124.2 (3)
Rh–C1–N	142.9 (3)	P–O23–C231	123.7 (3)
Rh′–C1–N	136.0 (3)	O11–C111–C113	106.7 (5)
C1–n–C2	139.3 (4)	O12–C121–C122	106.7 (6)
N–C2–C3	122.8 (4)	N12–C121–C123	109.1 (7)
N–C2–C7	117.8 (4)	O13–C131–C132	107.0 (5)
C3–C2–C7	119.3 (4)	mO13–C131–C133	110.7 (5)
C2–C3–C4	120.4 (4)	O21–C211–C212	108.9 (5)
C3–C4–C5	119.4 (5)	O21–C211–C212	108.9 (5)
C4–C5–C6	121.0 (5)	O21–C211–C213	106.8 (5)
Cl–C5–C4	119.0 (5)	O22–C221–C222	110.9 (5)
Cl–C5–C6	120.0 (5)	O22–C221–C223	105.5 (4)
C5–C6–C7	120.2 (5)	O23–C231–C232	106.9 (6)
C6–C7–C2	119.6 (5)	O23–C231–C233	113.5 (7)
Rh–P1–O11	119.20 (11)	C112–C111–C113	112.9 (6)
Rh–P1–O12	115.15 (11)	C122–C121–C123	112.4 (7)
Rh–P1–O13	120.65 (11)	C132–C131–C133	112.3 (5)
Rh–P2–O21	115.50 (11)	C212–C211–C213	112.1 (5)
Rh–P2–O22	117.86 (13)	C222–C221–C223	112.1 (5)
Rh–P2–O23	120.62 (13)	C232–C231–C233	108.2 (6)

and angle formation are listed in Tables V–VII. Perspective views of the molecule are shown in Figures 6 and 7. The molecule has crystallographically imposed symmetry due to a 2-fold axis that bisects the Rh–Rh vector. The observed diamagnetism of the compound requires a formal single bond between the two Rh atoms (both d^9). This is consistent with the Rh–Rh separation of 2.640 (1) Å. The two RhP1P2 planes are nearly orthogonal (dihedral angle 86.8°). The central $(\mu\text{-RNC})_2Rh_2$ unit is nonplanar, with a dihedral angle of 135.8° between the two RhRh′C planes; the N lies within 0.023 (4) Å of the RhRh′C plane. The RhRh′C planes lie at 24.7 and 111.4° angles to the RhP1P2 planes, so the geometry at Rh is neither planar nor tetrahedral (ignoring the Rh–Rh bond); indeed, it has no simple polyhedral description. In these respects, the structure is quite similar to that of the two related compounds, $(\mu\text{-CO})_2Rh_2[P(O\text{-}i\text{-}Pr)_3]_4$[8] and $(\mu\text{-CO})_2Rh_2(PPh_3)_4$,[30] both of which also display crystallographically imposed 2-fold symmetry. The isocyanides are bent at the nitrogen (C1–N–C2 = 139.3 (4)°). The Rh–C distances anti to the aryl groups are slightly shorter the the syn Rh–C distances, as has been noted for other compounds.[21-25] The aromatic rings are tilted slightly out of conjugation with the formal Cl=N double bond (the dihedral angle between the aromatic ring, which is planar to within 0.02 Å, and the C1–N–C2 plane is 18.2°), probably due to steric interactions with the phosphite alkyl groups.

It is interesting to note that in the solid-state structure there are two distinct phosphite environments: P1 and P1′ are on a different side of the bent $(\mu\text{-RNC})_2Rh_2$ core from P2 and P2′. This can best be seen in the view down the Rh–Rh bond in Figure 7. The two environments can easily be interconverted by a simple "flapping" motion of the isocyanide "wings" of the butterfly-shaped core, as shown in Figure 8. At room temperature, the $^{31}P\{^1H\}$ spectrum of **2a** appears as an AA′A″A‴XX′ pattern, indicating that the fluxional process is fast on the NMR time scale. At −70 °C, the spectrum is a featureless lump with a width of 4.5 ppm at 202.5 MHz. At −105 °C, two resonances are observed, at δ 158.2 and 139.9, corresponding to the two distinct environments expected. The resonances are still too broad at this temperature to resolve the coupling patterns, which are undoubtedly complex.

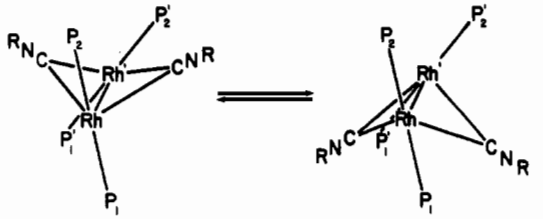

Figure 8. A fluxional process that interconverts the two phosphite environments in **2a**.

A simple coalescence-temperature approximation[31] ($k = 2^{-1/2}\pi(\Delta\nu)$, where $\Delta\nu$, the chemical shift difference in hertz, is assumed to be equal to its value estimated from the −95 °C spectrum) gives a $\Delta G^{\ddagger}$ of 8.1 kcal/mol at −70 °C for the process. The same process undoubtedly occurs for $(\mu\text{-CO})_2Rh_2P_4$ (P = $P(O\text{-}i\text{-}Pr)_3$, PPh_3) as well, but was not investigated in either case. The $^{31}P\{^1H\}$ NMR spectrum of $(\mu\text{-CO})_2Rh[P(O\text{-}i\text{-}Pr)_3]_4$ broadened only slightly at −98 °C, however, suggesting that the barrier is very low for this compound compared to its $4\text{-}ClC_6H_4NC$ analogue.

Analogy to CO Chemistry. Scheme II shows the overall course of the reactions of $(\mu\text{-H})_2Rh_2[P(O\text{-}i\text{-}Pr)_3]_4$ with isocyanides. Reaction of $(\mu\text{-H})_2Rh_2[P(O\text{-}i\text{-}Pr)_3]_4$ with a single equivalent of isocyanide leads to $(\mu\text{-H})_2(RNC)Rh_2[P(O\text{-}i\text{-}Pr)_3]_4$ (**1**). This compound can react further with isocyanide to yield $(\mu\text{-RNC})_2Rh_2[P(O\text{-}i\text{-}Pr)_3]_4$ (**2**), $HRh[P(O\text{-}i\text{-}Pr)_3]_3(RNC)$, or other products, depending on the isocyanide. The electronic nature of the isocyanide seems to be important in determining the product distribution. The highly electron-withdrawing $4\text{-}ClC_6H_4NC$ gave mainly **2a** while the electron-donating *t*-BuNC gave mainly $HRh[P(O\text{-}i\text{-}Pr)_3]_3(RNC)$; $PhCH_2NC$ and *n*-BuNC were intermediate in their behavior. Complex **1a** was so reactive toward additional $4\text{-}ClC_6H_4NC$ that it alone of all the isocyanide adducts could not be prepared in relatively pure form by reaction of $(\mu\text{-H})_2Rh_2[P(O\text{-}i\text{-}Pr)_3]_4$ with 1 equiv of RNC; the standard preparative method always resulted in further reaction of 10–20% of the **1a** with $4\text{-}ClC_6H_4NC$, displacing H_2 and forming **2a**. Thus the final product mixture contained **1a**, **2a**, unreacted $(\mu\text{-H})_2Rh_2[P(O\text{-}i\text{-}Pr)_3]_4$, and products resulting from the attack of H_2 on the first two compounds.[32] This resulted in a lower overall yield of **1a** than was observed for **1b–e**.

These observations suggested that the CO analogue, $(\mu\text{-H})_2(CO)Rh_2[P(O\text{-}i\text{-}Pr)_3]_4$, might not be unstable with respect to $(\mu\text{-CO})_2Rh_2[P(O\text{-}i\text{-}Pr)_3]_4$, as previously proposed,[8] but simply very sensitive to additional CO. This turned out to be the case. Reaction of $(\mu\text{-H})_2Rh_2[P(O\text{-}i\text{-}Pr)_3]_4$ with a single equivalent of CO under the same conditions used for the isocyanides resulted in a stable mixture of $(\mu\text{-H})_2(CO)Rh_2[P(O\text{-}i\text{-}Pr)_3]_4$ and $(\mu\text{-CO})_2Rh_2[P(O\text{-}i\text{-}Pr)_3]_4$ in a rougly 2:1 ratio (as determined by $^{31}P\{^1H\}$ NMR). The mixture could be obtained as an orange solid, but repeated recrystallization from a variety of solvent mixtures failed to change the ratio appreciably. Due to the difficulty in separating the two compounds, a more efficient way to prepare $(\mu\text{-H})_2(CO)Rh_2[P(O\text{-}i\text{-}Pr)_3]_4$ was developed. Instead of adding all of the CO at once, only $^1/_4$ equiv of CO was added to a solution of $(\mu\text{-H})_2Rh_2[P(O\text{-}i\text{-}Pr)_3]_4$. The product $(\mu\text{-H})_2(CO)Rh_2[P(O\text{-}i\text{-}Pr)_3]_4$ was then extracted, and the unreacted starting material was subjected to further fractional equivalents of CO. In this manner the buildup of $(\mu\text{-H})_2(CO)Rh_2[P(O\text{-}i\text{-}Pr)_3]_4$ in the reaction mixture was lessened, minimizing the production of $(\mu\text{-CO})_2Rh_2[P(O\text{-}i\text{-}Pr)_3]_4$. Even so, the eventual product from this method was contaminated with ca. 10% of $(\mu\text{-CO})_2Rh_2[P(O\text{-}i\text{-}Pr)_3]_4$ after recrystallization. Nevertheless, this provided a useful source of $(\mu\text{-H})_2(CO)Rh_2[P(O\text{-}i\text{-}Pr)_3]_4$ for comparison with its isocyanide analogues.

A central question is whether the structure of $(\mu\text{-H})_2(CO)Rh_2[P(O\text{-}i\text{-}Pr)_3]_4$ in solution is symmetrical, as suggested in ref

(30) (a) Singh, P.; Damann, C. B.; Hodgson, D. J. *Inorg. Chem.* **1973**, *12*, 1335. (b) Evans, D.; Yagupsky, G.; Wilkinson, G. *J. Chem. Soc. A* **1968**, 2660.

(31) Sandstrom, J. *Dynamic NMR Spectroscopy*. Academic: New York, 1982.

(32) McKenna, S. T.; Andersen, R. A.; Muetterties, E. L. *Organometallics* **1986**, *5*, 2233.

8, or unsymmetrical, like its isocyanide analogues. The answer to this question should be found in the low-temperature $^{31}P\{^1H\}$ NMR; a symmetrical structure would give a temperature-invariant $^{31}P\{^1H\}$ spectrum. The spectrum was found to broaden at low temperatures in the same unsymmetrical fashion as the isocyanide compounds. As with the 2,6-$Me_2C_6H_3NC$ complex **1e**, however, fluxionality proved to be so facile that a low-temperature limit could not be reached. The $^{31}P\{^1H\}$ NMR spectrum of $(\mu\text{-H})_2(CO)Rh_2[P(O\text{-}i\text{-}Pr)_3]_4$ at −98 °C resembled that of **1e** at −90 °C and the *n*-BuNC analogue **1c** at −60 °C. Therefore the structure of $(\mu\text{-H})_2(CO)Rh_2[P(O\text{-}i\text{-}Pr)_3]_4$ is similar to that of the isocyanide compounds; its IR spectrum shows that the CO probably bridges the distinct rhodium atoms, like the isocyanides in **1–c**. Assuming that the chemical shift differences between ^{31}P environments are similar to those in the isocyanide compounds, its barrier to fluxionality is slightly lower than that of **1e**. This goes against the trend observed for the isocyanides, where less sterically demanding ligands led to higher barriers, and suggests that electronic factors can be important as well. The energy of the transition state in Figure 4, which has a symmetrically bridging RNC (or CO), should be lowered for a more electron-withdrawing, and therefore better bridging, ligand. Apparently the electronic differences between the isocyanides are not sufficiently large to outweight steric factors, while the electronic difference between isocyanides and the much more electron-withdrawing CO overcomes the effect of CO's small size.

Conclusion

The reaction of $(\mu\text{-H})_2Rh_2[P(O\text{-}i\text{-}Pr)_3]_4$ with isocyanides has been shown to produce a series of monoadducts $(\mu\text{-H})_2(RNC)Rh_2[P(O\text{-}i\text{-}Pr)_3]_4$ with an unsymmetrical structure. The details of the structure, specifically the degree of bridging displayed by the isocyanide ligand, are mainly a function of the size of the isocyanide; steric interactions force large isocyanides into a near-terminal configuration, while smaller ligands are closer to a bridging position. The adducts appear symmetrical on the NMR time scale at room temperature due to a fluxional process that allows the isocyanide to move from one rhodium atom to the other; the barrier for this process decreases with increasing steric bulk of the isocyanide due to steric destabilization of the ground state relative to the transition state. Carbon monoxide forms an analogous adduct with an unsymmetrical but bridging structure, as expected from its small size, but it displays a very low barrier to fluxionality due to its far greater electron-withdrawing ability compared to that of the isocyanides. Reaction of the monoadducts with additional RNC or CO gives different products depending on the ligand used. Highly electron-withdrawing CO or 4-ClC_6H_4NC leads mainly to $(\mu\text{-L})_2Rh_2[P(O\text{-}i\text{-}Pr)_3]_4$, while other, more electron-donating isocyanides give fragmentation to $HRh[P(O\text{-}i\text{-}Pr)_3]_3(RNC)$ and other products.

The variability of steric and electronic factors possible with isocyanides has thus proved to be useful in investigating trends of structure and reactivity in the coordination chemistry of $(\mu\text{-H})_2Rh_2[P(O\text{-}i\text{-}Pr)_3]_4$. It may be noted that the reactivity of $(\mu\text{-H})_2Rh_2[P(O\text{-}i\text{-}Pr)_3]_4$ with phosphites and acetylenes may be rationalized by using these trends. Disubstituted acetylenes, good bridging ligands that have only small steric requirements when coordinated perpendicular to the Rh–Rh vector, react with $(\mu\text{-H})_2Rh_2[P(O\text{-}i\text{-}Pr)_3]_4$ to form, initially, strong adducts with retention of the binuclear structure. Phosphites, on the other hand, are more sterically demanding and cannot provide structural stability by bridging; therefore, they cause fragmentation. The steric and electronic trends affecting the further reactivity of the isocyanide compounds will be explored in a another paper.[32]

Experimental Section

Reagents and Methods. All manipulations were performed by using standard Schlenk techniques or in a Vacuum Atmospheres drybox under argon or nitrogen. Toluene, pentane, and tetrahydrofuran were distilled from sodium/benzophenone. Acetonitrile was distilled from P_4O_{10} onto freshly activated 3-Å molecular sieves and then distilled again. 2-Propanol was dried with 3-Å molecular sieves or with sodium 2-propoxide and distilled. Deuteriated solvents were stored over sodium/potassium/benzophenone and vacuum distilled directly into the NMR tube before sealing. The $P(O\text{-}i\text{-}Pr)_3$ was stored over sodium for one week and then fractionally distilled under reduced pressure. The isocyanides *t*-BuNC, *n*-BuNC, and $PhCH_2NC$ were vacuum distilled before use. The 4-ClC_6H_4NC and 4-$O_2NC_6H_4NC$ were prepared from the corresponding anilines[33] and sublimed immediately before use. Ethylene and carbon monoxide (Matheson), $RhCl_3\cdot 3H_2O$ (Johnson Matthey/Aesar), 2,6-$Me_2C_6H_3NC$ (Fluka), and $KBH(O\text{-}i\text{-}Pr)_3$ (1.00 M in THF, Aldrich) were used as received.

The ^1H, ^{31}P, and ^{13}C NMR spectra were recorded on 180-, 200-, 250-, or 300-MHz (proton) instruments, consisting of Oxford superconducting magnets interfaced to Nicolet computers, or on a Bruker AM-500 instrument. The ^1H and ^{13}C spectra were referenced to tetramethylsilane. The ^{31}P spectra were referenced to external $P(OMe)_3$ and later corrected to 85% H_3PO_4. Positive chemical shifts are downfield in all cases and are expressed in δ. IR spectra were taken on a Perkin-Elmer 283 spectrophotometer. Mass spectra were obtained via electron impact (70 eV) using an AEI MS-12 instrument with an INCOS data system. Elemental analyses were performed by Vazken H. Tashinian in the UC Berkeley Microanalytical Laboratory.

$(\mu\text{-H})_2Rh_2[P(O\text{-}i\text{-}Pr)_3]_4$. This compound was prepared by a modification of the previously published procedure.[6] To a solution of 3.42 g (3.08 mmol) of $(\mu\text{-Cl})_2Rh_2[P(O\text{-}i\text{-}Pr)_3]_4$[29] in 100 mL of THF at −78 °C was added 6.5 mL (2.1 equiv) of a 1.00 M solution of $KBH(O\text{-}i\text{-}Pr)_3$ in THF via syringe under an argon atmosphere. The solution rapidly turned red. The cooling bath was removed, and the mixture was allowed to stir for 1–2 h. The color darkened to greenish black as the solution warmed to room temperature. Excess borohydride and $\{(\mu\text{-H})_3Rh_2[P(O\text{-}i\text{-}Pr)_3]_4^-\}$[7] were quenched by adding a few milliliters of degassed 2-propanol via syringe. The solution was evaporated to dryness, and the residue was taken up in pentane (ca. 100 mL). The mixture was filtered through a medium frit and again through a fine frit. The filtrate was reduced in volume to about 50 mL and cooled to −40 °C. Three crops of large green-black crystals were isolated and washed with cold pentane for a total of 1.80 g (56%). Spectroscopic data for this material were identical with those reported previously.[1]

$(\mu\text{-H})_2(t\text{-BuNC})Rh_2[P(O\text{-}i\text{-}Pr)_3]_4$ (1d). A solution of 50 μL (37 mg, 0.44 mmol) of *t*-BuNC in 20 mL of THF was added dropwise to a solution of 450 mg (0.43 mmol) of $(\mu\text{-H})_2Rh_2[P(O\text{-}i\text{-}Pr)_3]_4$ in 100 mL of THF at room temperature. The color changed immediately from green to red. The solution was evaporated to dryness, and the residue was dissolved in a minimum (ca. 10 mL) of 2:1 2-propanol/acetonitrile. Crystallization at −40 °C gave 425 mg (88%) of orange crystals after three crops. ^1H NMR (toluene-d_8): δ 5.00 (mult, 12 H), 1.44 (s, 9 H), 1.35 (d, J_{HH} = 6.2 Hz, 72 H); data for hydrides are given in Table I. ^{13}C NMR (3:2 THF-d_8/toluene-d_8, 10 °C): δ 155.35 (quin of t, J_{CP} = 41 Hz, J_{CRh} = 22 Hz, RN*C*), 66.93 (d, J_{CH} = 144.5 Hz, *C*HMe$_2$), 57.93 (s, *C*Me$_3$), 30.94 (quartet, J_{CH} = 127.8 Hz, C(*C*H$_3$)$_3$), 25.22 (quar, J_{CH} = 125.4 Hz, CH(*C*H$_3$)$_2$). Anal. Calcd for $C_{41}H_{95}NO_{12}P_4Rh_2$: C, 43.8; H, 8.52; N, 1.25; P, 11.0. Found: C, 43.9, H, 8.36; N, 1.30; P, 11.1. The other compounds of type **1** were prepared similarly.

$(\mu\text{-H})_2(PhCH_2NC)Rh_2[P(O\text{-}i\text{-}Pr)_3]_4$ (1b). This compound was isolated in 70% yield as red crystals. ^1H NMR (toluene-d_8): δ 7.49 (d, J_{HH} = 7.5 Hz, 2 H), 7.1 (mult, 3 H), 4.94 (mult, 12 H), 4.88 (s, 2 H), 1.32 (d, J_{HH} = 6.1 Hz, 72 H); data for hydrides are given in Table I. ^{13}C NMR (THF-d_8, 10 °C): δ 205.86 (quin of t, J_{CP} = 42.6 Hz, J_{CRh} = 26.5 Hz, RN*C*), 140.63 (s, ipso Ph), 128.52 (d, J_{CH} = 158.1 Hz, ortho or meta Ph), 127.77 (d, J_{CH} = 158.5 Hz, meta or ortho Ph), 126.76 (d, J_{CH} = 159.3 Hz, para Ph), 67.78 (d, J_{CH} = 144.9 Hz, *C*HMe$_2$), 53.05 (t, J_{CH} = 139.2 Hz, Ph*C*H$_2$), 25.16 (quar, J_{CH} = 125.5 Hz, CH(*C*H$_3$)$_2$). Anal. Calcd for $C_{44}H_{93}NO_{12}P_4Rh_2$: C, 45.6; H, 8.10; N, 1.21; P, 10.7. Found: C, 45.7; H, 8.12; N, 1.20; P, 10.6.

$(\mu\text{-H})_2(n\text{-BuNC})Rh_2[P(O\text{-}i\text{-}Pr)_3]_4$ (1c). This compound was isolated in 69% yield as orange crystals. ^1H NMR (toluene-d_8): δ 4.93 (mult, 12 H), 3.57 (t, J_{HH} = 7.3 Hz, 2 H, CNC*H*$_2$), 1.58 (mult, 2 H, CNCH$_2$C*H*$_2$), 1.45 (mult, 2 H, CNCH$_2$CH$_2$C*H*$_2$), 1.34 (d, J_{HH} = 6.2 Hz, 72 H), 0.93 (t, J_{HH} = 7.3 Hz, 3 H, CN(CH$_2$)$_3$C*H*$_3$); data for hydrides are given in Table I. Anal. Calcd. for $C_{41}H_{95}NO_{12}P_4Rh_2$: C, 43.8; H, 8.52; N, 1.25; P, 11.0. Found: C, 43.7; H, 8.80; N, 1.23; P, 11.3.

$(\mu\text{-H})_2(2,6\text{-}Me_2C_6H_3NC)Rh_2[P(O\text{-}i\text{-}Pr)_3]_4$ (1e). This compound was isolated in 58% yield as red crystals. ^1H NMR (toluene-d_8): δ 6.8 (mult, 3 H), 5.00 (mult, 12 H), 2.42 (s, 6 H), 1.29 (d, J_{HH} = 6.2 Hz, 72 H); data for hydrides are given in Table I. Anal. Calcd for $C_{45}H_{95}NO_{12}P_4Rh_2$: C, 46.1; H, 8.17; N, 1.20; P, 10.6. Found: C, 46.1; H, 8.30; N, 1.37; P, 10.4.

(33) Weber, W. P.; Gokel, G. W.; Ugi, I. K. *Angew. Chem., Int. Ed. Engl.* **1972**, *11*, 530.

$(\mu\text{-H})_2(4\text{-ClC}_6H_4NC)Rh_2[P(O\text{-}i\text{-Pr})_3]_4$ (1a) and $(\mu\text{-4-ClC}_6H_4NC)Rh_2[P(O\text{-}i\text{-Pr})_3]_4$ (2a). The reaction was performed as above except that the temperature was kept at −78 °C and a continuous flow of argon through the vessel was employed in order to help flush out any H_2 formed. After the product was extracted into 2-propanol/acetonitrile, the mixture was filtered and the recovered brown solid residue was set aside. The material obtained from crystallization of the filtrate (crude yield ca. 45%) was recrystallized from pure 2-propanol to give the product **1a** in 16% overall yield. ^{1}H NMR (toluene-d_8): δ 7.43 and 7.14 (AA′BB′ pattern, $|^3J_{AB} + {}^5J_{AB'}| = 8.5$ Hz, 4 H), 4.88 (mult, 12 H), 1.28 (d, $J_{HH} = 6.1$ Hz, 72 H); data for hydrides are given in Table I. Anal. Calcd. for $C_{43}H_{87}ClNO_{12}P_4Rh_2$: C, 43.8; H, 7.70; N, 1.19; P, 10.5; Cl, 3.01. Found: C, 44.1; H, 7.91; N, 1.43; P, 10.3; Cl, 3.11. The brown solid residue from the initial filtration was washed with pentane (ca. 10 mL) to remove $(\mu\text{-H})_2Rh_2[P(O\text{-}i\text{-Pr})_3]_4$. The remaining red powder was recrystallized from pentane to yield ca. 12% (based on Rh) of dark red crystals of **2a**. ^{1}H NMR (toluene-d_8): δ 7.40 and 7.17 (AA′BB′ pattern, $|^3J_{AB} + {}^5J_{AB'}| = 8.6$ Hz, 8 H), 4.79 (mult, 12 H), 1.24 (d, $J_{HH} = 6.1$ Hz, 72 H). ^{31}P{^{1}H} NMR (toluene-d_8): δ 148.0 (AA′A″A‴XX′ pattern, $^1J_{PRh} = 269.4$ Hz, $^3J_{PRh} = 5.5$ Hz, $J_{RhRh} = 73.1$ Hz). IR (pentane): 1690 cm^{-1} (ν_{CN}). Anal. Calcd for $C_{50}H_{92}Cl_2N_2O_{12}P_4Rh_2$: C, 45.7; H, 7.06; N, 2.13; P, 5.40; Cl, 9.43. Found: C, 45.5; H, 7.15; N, 2.28; P, 5.15; Cl, 9.14.

Dynamic NMR of 1a–e. Spectra were recorded of solutions in THF-d_8 or 3:2 THF-d_8/toluene-d_8 at 5–10 °C intervals over the temperature range of approximately −105 to 0 °C. The combination of limiting high- and low-temperature spectra was sufficient to derive most parameters to a precision of a few hertz or better. The exception was $^2J_{PP}$, which was unobservable due to magnetic equivalence (real or effective) in the high-temperature limit and unobservable as $^2J_{P3P4}$ in the low-temperature limit. Since $^2J_{P1P2}$ was observable, $^2J_{P3P4}$ was set to the same value. Chemical shifts were read from the low-temperature spectra, and where possible (**1a**,**c**), the temperature dependence of the individual chemical shifts were measured and extrapolated linearly to higher temperatures; this was found to closely predict the averaged chemical shift of the high-temperature limiting spectra. For **1b** and **1d**, sufficient data below the low-temperature limit were not available and the observed frequency differences were held constant, with only the average being varied linearly. Calculations were performed by using DYNAMAR, a locally modified version of a mutual exchange program originally written by Meakin,[34] and visually matched to observed spectra. Two equivalent permutations were used, corresponding to the two possible directions of rotation of RNC about the Rh–Rh vector, each proceeding at rate $k/2$. Data were fitted to the Eyring equation by using weighted least squares by the program ACTPAR of Binsch.[35]

$HRh[P(O\text{-}i\text{-Pr})_3]_3(t\text{-BuNC})$. To 1.18 g (1.62 mmol) of $HRh[P(O\text{-}i\text{-Pr})_3]_3$ (from $ClRh[P(O\text{-}i\text{-Pr})_3]_3$ and $KBH(O\text{-}i\text{-Pr})_3$)[7] in 100 mL of pentane was added a solution of 0.190 mL (1.68 mmol) of *t*-BuNC in 25 mL of pentane dropwise over 20 min. The solution was stirred for 1 h at room temperature and then evaporated to dryness. Crystallization at −40 °C from 4:1 2-propanol/acetonitrile gave 745 mg (56%) of a light yellow powder. ^{1}H NMR (toluene-d_8): δ 4.91 (mult, 9 H), 1.32 (d, $J_{HH} = 6.2$ Hz, 54 H), 1.22 (s, 9 H), −12.73 (quar of d, $J_{HP} = 12.5$ Hz, $J_{HRh} = 6.9$ Hz, 1 H). ^{31}P{^{1}H} NMR (toluene-d_8): δ 162.0 (d, $J_{PRh} = 224.9$ Hz). IR (pentane): 2130 (ν_{CN}), 1700 cm^{-1} (weak, *ca.* 100 cm^{-1} wide, ν_{HRh}). Mass spectrum, *m/e* 811 (M+); ions due to losses of *t*-BuNC, $P(O\text{-}i\text{-Pr})_3$, OC_3H_7, and C_6H_8. Anal. Calcd for $C_{32}H_{73}NO_9P_3Rh$: C, 47.4; H, 9.06; N, 1.73; P, 11.4. Found: C, 47.5; H, 9.20; N, 1.68; P, 11.5.

Reactions of 1 with RNC. In a typical experiment, 30 mg of **1** was dissolved in ca. 20 mL of THF. A solution of 1.1–1.5 equiv of the appropriate RNC in 10 mL of THF was added over the course of 1 min. The solution was stirred at room temperature for 2–4 h. The volume was reduced to ca. 2 mL; the solution was transferred by cannula to an NMR tube attached to a Teflon valve, and the remaining solvent was removed under reduced pressure. Deuteriated solvent was then transferred into the NMR tube, and it was sealed. For R = *n*-Bu, the reaction started with $(\mu\text{-H})_2Rh_2[P(O\text{-}i\text{-Pr})_3]_4$ and 2.8 equiv. of *n*-BuNC. Data for **2a** and $HRh[P(O\text{-}i\text{-Pr})_3]_3(t\text{-BuNC})$ are given above. Data for other compounds detected in this manner but not isolated are given below.

$HRh[P(O\text{-}i\text{-Pr})_3]_3(n\text{-BuNC})$. ^{1}H NMR (toluene-$d_8$): δ −12.69 (quar of d, $J_{HP} = 11.6$ Hz, $J_{HRh} = 6.9$ Hz). ^{31}P{^{1}H} NMR (toluene-d_8): δ 162.2 (d, $J_{PRh} = 224.8$ Hz).

$HRh[P(O\text{-}i\text{-Pr})_3]_3(4\text{-ClC}_6H_4NC)$. ^{1}H NMR (toluene-$d_8$): δ −11.74 (quar of d, $J_{HP} = 10.7$ Hz, $J_{HRh} = 5.9$ Hz). ^{31}P{^{1}H} NMR (toluene-d_8): δ 161.2 (d, $J_{PRh} = 222.4$ Hz).

$HRh[P(O\text{-}i\text{-Pr})_3]_3(PhCH_2NC)$. ^{1}H NMR (toluene-$d_8$): δ −12.49 (quar of d, $J_{HP} = 11.4$ Hz, $J_{HRh} = 6.8$ Hz). ^{31}P{^{1}H} NMR (toluene-d_8): δ 162.0 (d, $J_{PRh} = 224.3$ Hz).

$(\mu\text{-PhCH}_2NC)_2Rh_2[P(O\text{-}i\text{-Pr})_3]_4$ (2b). ^{31}P{^{1}H} NMR (toluene-d_8): δ 151.0 (AA′A″A‴XX′ pattern, $|^1J_{PRh} + {}^3J_{PRh}| = 275.1$ Hz, $J_{RhRh} = 67$ Hz).

$(\mu\text{-H})_2(CO)Rh_2[P(O\text{-}i\text{-Pr})_3]_4$. A solution of 600 mg (0.576 mmol) of $(\mu\text{-H})_2Rh_2[P(O\text{-}i\text{-Pr})_3]_4$ in 25 mL of toluene in a Schlenk tube was cooled to 0 °C. The tube was isolated from the Schlenk line, and 3.5 mL (0.25 equiv assuming ideal gas behavior) of CO was injected into the vapor phase above the solution via a gastight syringe while the mixture was rapidly stirred. The solution color turned immediately to greenish red. After the mixture was stirrred for 5 min, the solution was evaporated to dryness. The residue was washed with 20 mL of 1:1 acetonitrile/2-propanol and filtered through a cannula filter. The orange filtrate was set aside, while the green solid residue was redissolved in toluene. This procedure was repeated for four more additions (of 3.5, 2.3, 1.6, and 1.0 mL) of CO for a total of 11.9 mL (0.85 equiv). The combined filtrates were evaporated to dryness and crystallized from ca. 15 mL of 10:1 acetonitrile/2-propanol at −40 °C. Two crops gave 383 mg (62% based on Rh, 73% based on CO) of orange crystals. IR and ^{31}P{^{1}H} NMR showed the product to be 90% $(\mu\text{-H})_2(CO)Rh_2[P(O\text{-}i\text{-Pr})_3]_4$ and 10% $(\mu\text{-CO})_2Rh[P(O\text{-}i\text{-Pr})_3]_4$. Anal. Calcd for pure $(\mu\text{-H})_2(CO)Rh_2[P(O\text{-}i\text{-Pr})_3]_4$, $C_{37}H_{86}O_{13}P_4Rh_2$: C, 41.6; H, 8.11; P, 11.6. Found: C, 41.5; H, 8.13; P, 11.5. Data for $(\mu\text{-H})_2(CO)Rh_2[P(O\text{-}i\text{-Pr})_3]_4$: ^{1}H NMR (toluene-$d_8$): δ 4.93 (mult, 12 H), 1.32 (d, $J_{HH} = 6.2$ Hz, 72 H), −9.09 (quin of t, $J_{HP} = 47.2$ Hz, $J_{HRh} = 14.0$ Hz, 2 H). Data for $(\mu\text{-CO})_2Rh_2[P(O\text{-}i\text{-Pr})_3]_4$: ^{1}H NMR (toluene-$d_8$): δ 4.93 (mult, 12 H), 1.33 (d, $J_{HH} = 6.2$ Hz, 72 H). ^{31}P{^{1}H} NMR (toluene-d_8): δ 151.6 (AA′A″A‴XX′ pattern, $|^1J_{PRh} + {}^3J_{PRh}| = 287.3$ Hz, $J_{RhRh} = 76.6$ Hz). Other data are given in ref 8.

X-ray Crystallographic Study of $(\mu\text{-4-ClC}_6H_4NC)_2Rh_2[P(O\text{-}i\text{-Pr})_3]_4$ (2a). Dark red crystals were grown by cooling a saturated solution in pentane to −40 °C. The crystal selected was shaped roughly like an octahedron elongated and truncated along one axis and was bounded by faces of the form (001), (11$\bar{1}$), (1$\bar{1}\bar{1}$), (110), and (1$\bar{1}$0). The crystal was mounted in a glass capillary and sealed under nitrogen. Precession photographs indicated monoclinic symmetry and systematic absences consistent with the space groups $C2/c$ and Cc. The choice of the former is supported by intensity statistics and by the presence of the appropriate Harker vectors in the Patterson map and confirmed by the successful solution of the structure. The final cell parameters were determined from a least-squares fit of 24 well-centered reflections with $2\theta \sim 28°$. Intensity data were collected using the parameters listed in Table IV. Crystal orientation was checked by using three reflections measured every 300 data; reorientation was not required during data collection. The intensities of the same three reflections were monitored every hour of X-ray exposure to check for decay. A linear, isotropic decay totaling 3% was observed along with a one-time 6% step increase in generator output after approximately 900 reflections. Both were corrected for along with Lorentz and polarization effects. Azimuthal scans of five reflections with high χ showed I_{min}/I_{max} averaging 0.97; this was judged to be insufficient to warrant attempting to correct for absorption. The position of the rhodium atom was deduced from the Patterson map and all other atoms were located by standard least-squares and Fourier techniques. After refinement of all non-hydrogen atoms with anisotropic thermal parameters, a difference Fourier map showed peaks for most of the hydrogen atoms. At this point all hydrogen atoms were inserted in idealized positions with a C–H bond length of 0.95 Å and given isotropic thermal parameters (B's) 1 Å^2 greater than the equivalent isotropic thermal parameter of the attached carbon. Hydrogen atoms were included in structure factor calculations but not refined. Full-matrix nonlinear least-squares methods were used, the function minimized being $\sum w(|F_o| - |F_c|)^2$, where the weight of a given observation $w = 4F_o^2/[\sigma_o^2(F_o^2) + (pF_o^2)^2]$ with $p = 0.04$. The analytical forms of the scattering factor tables were used and all non-hydrogen scattering factors were corrected for the real and imaginary components of anomalous dispersion. Examination of F_o vs. F_c for the 25 most intense reflections suggested no effects due to secondary extinction; inspection of the final residuals with respect to ranges of parity, F_o, (sin θ/λ, hkl, and various projections revealed no unusual trends. Refinement continued until the largest shift/error was less than 0.01. The largest peaks in the final difference Fourier map corresponded to 0.2 e/Å^3 and were located near phosphite oxygens. All calculations were performed by using programs from the Enraf-Nonius SDP package.

***trans*-$RhCl[P(O\text{-}i\text{-Pr})_3]_2(PhCH_2NC)$.** To a solution of 1.00 g (0.901 mmol) of $(\mu\text{-Cl})_2Rh_2[P(O\text{-}i\text{-Pr})_3]_4$[29] in pentane was added 219 μL (0.211 g, 1.80 mmol) of $PhCH_2NC$ via syringe. The resulting light yellow solution was filtered and concentrated. Slow cooling to −70 °C gave 0.995 g (82%) of light yellow crystals. ^{1}H NMR (THF-d_8): δ 7.43 (d,

(34) Meakin, P.; Muetterties, E. L.; Tebbe, F. N.; Jesson, J. P. *J. Am. Chem. Soc.* **1971**, *93*, 4701.
(35) Binsch, G.; Kessler, H. *Angew. Chem., Int. Ed. Engl.* **1980**, *19*, 411.

J = 7.4 Hz, 2 H, ortho), 7.35 (t, 2 H, meta), 7.28 (t, 1 H, para), 5.13 (mult, 6 H), 4.70 (s, 2 H, $PhCH_2$), 1.25 (d, J = 6.2 Hz, 36 H). ^{13}C NMR (THF-d_8): δ 155.20 (d of t, J_{CRh} = 69.3 Hz, J_{CP} = 21.0 Hz, RNC), 132.82 (s, ipso Ph), 129.4 (d of d, $^1J_{CH}$ = 160.7 Hz, $^2J_{CH}$ = 7.5 Hz, ortho Ph), 128.55 (d of t, $^1J_{CH}$ = 161.2 Hz, $^2J_{CH}$ = 7.1 Hz, para Ph), 127.31 (d of mult, $^1H_{CH}$ = 159.6, meta Ph), 69.23 (d, $^1J_{CH}$ = 146.7 Hz, $CHMe_2$), 47.92 (t, $^1J_{CH}$ = 143.6 Hz, $PhCH_2$), 24.81 (quar of virtual t, $^1J_{CH}$ = 125.6 Hz, $|^3J_{CP} + {}^5J_{CP}|$ = 3.7 Hz, $CH(CH_3)_2$). $^{31}P\{^1H\}$ NMR (THF-d_8): 127.7 (d, J_{PRh} = 202.1 Hz). IR (pentane): 2130 cm^{-1} (ν_{CN}). Anal. Calcd for $C_{26}H_{49}ClNO_6P_2Rh$: C, 46.5; H, 7.35; N, 2.08; P, 9.22; Cl, 5.28. Found: C, 46.7; H, 7.32; N, 2.12; P, 9.38; Cl, 5.43.

***trans*-RhCl[P(O-*i*-Pr)$_3$]$_2$(4-ClC$_6$H$_4$NC).** Preparation was similar to that of the $PhCH_2NC$ analogue; it was isolated in 92% yield as light yellow crystals. ^1H NMR (C_6D_6): δ 6.88 and 6.74 (AA'BB' pattern, $|^3J_{AB} + {}^5J_{AB'}|$ = 8.7 Hz, 4 H), 5.42 (septet of virtual t, J_{HH} = 6.2 Hz, $|^3J_{HP} + {}^5J_{HP}|$ = 9.7 Hz, 6 H), 1.34 (d, J_{HH} = 6.2 Hz, 36 H). $^{13}C\{^1H\}$ NMR (C_6D_6): δ 131.88 and 130.40 (ipso and para Ph), 129.41 and 126.54 (ortho and meta Ph), 69.32 ($CHMe_2$), 24.60 ($CH(CH_3)_2$); RNC not observed. $^{31}P\{^1H\}$ NMR (C_6D_6): δ 126.1 (d, J_{PRh} = 200.0 Hz). IR (pentane): 2098 cm^{-1} (ν_{CN}).

Acknowledgment. This work was sponsored by the National Science Foundation in the form of a research grant (No. CHE 830-7159) and a predoctoral fellowship for S.T.M. We thank Dr. Frederick J. Hollander of the UC Berkeley X-ray crystallographic facility (CHEXRAY) for assistance with the crystal structure of **2a**, and Prof. Richard A. Andersen for his guidance. Johnson Matthey Inc. provided a generous loan of $RhCl_3 \cdot 3H_2O$.

Supplementary Material Available: Tables of anisotropic thermal parameters for non-hydrogen atoms, hydrogen atom positions, and isotropic thermal parameters for **2a** (4 pages); a table of observed and calculated structure factors for **2a** (17 pages). Ordering information is given on any current masthead page.

Contribution from the Department of Chemistry and Laboratory for Molecular Structure and Bonding, Texas A&M University, College Station, Texas 77843

Conversion of an Electron-Rich Triple Bond to a Double Bond by Oxidative Addition of Diphenyl Diselenide to $Re_2Cl_4(\mu\text{-dppm})_2$. Preparation and Characterization of $Re_2Cl_4(\mu\text{-SePh})_2(\mu\text{-dppm})_2$ (dppm = Bis(diphenylphosphino)methane)

F. Albert Cotton* and Kim R. Dunbar

Received September 24, 1986

The dirhenium(II) complex $Cl_2Re(\mu\text{-dppm})_2ReCl_2$ with a $\sigma^2\pi^4\delta^2\delta^{*2}$ triple bond undergoes a clean, facile reaction with PhSeSePh to produce $Cl_2Re(\mu\text{-SePh})_2(\mu\text{-dppm})_2ReCl_2$ in high yield. In this reaction, oxidative addition of the Se–Se single bond to the Re≡Re triple bond results in a conversion of the d^5–d^5 M_2L_8 parent compound to a d^4–d^4 M_2L_{10} species which possesses a formal double bond ($\sigma^2\pi^2\delta^{*2}\delta^2$). The identity of the product has been confirmed by a single-crystal X-ray study, and the structural results are compared with the data previously reported for the analogous doubly bonded $Re_2Cl_6(dppm)_2$. $Re_2Cl_4(SePh)_2(dppm)_2$ crystallizes in the monoclinic space group $P2_1/n$ with a = 13.115 (2) Å, b = 15.463 (5) Å, c = 14.309 (2) Å, β = 102.00 (1)°, V = 2838 (2) Å^3, and Z = 2. The crystallographic symmetry of the molecule is $\bar{1}$ while the effective molecular symmetry is $2/m$ (C_{2h}). Important bond distances and angles are Re–Se(av) = 2.462 [1] Å, Re–Cl(av) = 2.45 [1] Å, Re–P(av) = 2.474 [9] Å, ∠Re–Re–Se = 57.33 (4)°, and ∠Re–Re–Cl(av) = 140.4 [1]°. The Re–Re distance in $Re_2Cl_4(SePh)_2(dppm)_2$ is 2.656 (1) Å, which is 0.04 Å longer than the M–M distance in $Re_2Cl_6(dppm)_2$. The lengthening of the Re–Re bond is attributed to the difference in size of the bridging groups (SePh vs. Cl). The properties of the title compound were investigated by several other methods, including infrared and UV–visible spectroscopy and electrochemistry. The near-infrared spectrum of $Re_2Cl_4(SePh)_2(dppm)_2$ exhibits a broad band at 1480 nm ($\epsilon \simeq 200$), a feature that is also found in the electronic spectrum of $Re_2Cl_6(dppm)_2$. A cyclic voltammetric study revealed the presence of four reversible one-electron redox couples; two couples located at $E_{1/2}$ = +0.95 and +1.65 V vs. Ag/AgCl correspond to oxidation processes, and two couples at $E_{1/2}$ = −0.46 and −1.30 V represent reductions. These metal-based redox properties are very similar to those observed for $Re_2Cl_6(dppm)_2$, $Re_2Cl_4(CO)_2(dppm)_2$, and other related dirhenium complexes with an edge-sharing bioctahedral geometry.

Introduction

The cleavage and substitution chemistry of binuclear compounds containing multiple metal–metal bonds is well-documented.[1] A much less developed facet of the reactivity of these complexes is their tendency to oxidatively add a substrate across the unsaturated M–M unit. Current work in these laboratories is directed toward a thorough investigation of the oxidative-addition chemistry of double ($\sigma^2\pi^2$), triple ($\sigma^2\pi^4$ and $\sigma^2\pi^4\delta^2\delta^{*2}$), and quadruple ($\sigma^2\pi^4\delta^2$) bonds. A primary objective in pursuing these studies is the development of high-yield, rational syntheses of edge-sharing bioctahedral complexes. Some results that have appeared in the literature include the reactions of disulfides (RSSR) with the double bond of $Ta_2Cl_6(Me_2S)_3$[2] and with the quadruple bond of $Mo_2Cl_4(L\text{-}L)_2$[3,4] compounds to yield the thiolate-bridged M_2L_{10} complexes $(Me_2S)Cl_3Ta(\mu\text{-SEt})_2TaCl_3(Me_2S)$ and (L-L)-$Cl_2Mo(\mu\text{-SR})_2MoCl_2$(L-L) (R = Et, L-L = 1,2-bis(dimethylphosphino)ethane (dmpe), 4,7-dithiadecane (dtd); R = Ph, L-L = dmpe, dtd, 3,6-dithiaoctane (dto)). These interesting compounds possess unusual electronic properties, and a few of them have been subjected to in-depth structural, magnetic, and theoretical studies.

The promising nature of the oxidative-addition reactions involving double, quadruple, and electron-poor triple bonds prompted us to extend our studies by probing the reactivity of the electron-rich triple bond as found in the coordinatively unsaturated dirhenium(II) compounds. Preliminary results from the reactions of $Re_2Cl_4(\mu\text{-dppm})_2$ with halogens, disulfides, and diselenides indicate that a smooth addition occurs which converts the parent $Re^{II}Re^{II}$ complex to a $Re^{III}Re^{III}$ species. The doubly bonded $Re_2Cl_4(\mu\text{-SePh})_2(\mu\text{-dppm})_2$ with bridging SePh groups was prepared via reaction of PhSeSePh with $Re_2Cl_4(dppm)_2$. The structural, spectroscopic, and electrochemical properties of the product are presented in this paper. This result represents the first instance in which a d^4–d^4 M_2L_{10} complex has been prepared from a d^5–d^5 M_2L_8 compound. The approach takes advantage of the facile oxidation of the $\sigma^2\pi^4\delta^2\delta^{*2}$ bond, and it is a superior method for the designed synthesis of new edge-sharing bioctahedral

(1) Cotton, F. A.; Walton, R. A. *Multiple Bonds between Metal Atoms*; Wiley: New York, 1982, and references therein.
(2) Campbell, G. C.; Canich, J. M.; Cotton, F. A.; Duraj, S. A.; Haw, J. F. *Inorg. Chem.* **1986**, *25*, 287.
(3) Cotton, F. A.; Powell, G. L. *J. Am. Chem. Soc.* **1984**, *106*, 3371.
(4) Cotton, F. A.; Diebold, M. P.; O'Connor, C. J.; Powell, G. L. *J. Am. Chem. Soc.* **1985**, *107*, 7438.

0020-1669/87/1326-1305$01.50/0